Int. J. Multiphase Flow Vol. 4, pp. 323–337

0301-9322/78/0601-0323/$02.00/0

A TWO-FLUID MODEL FOR CRITICAL VAPOUR–LIQUID FLOW

K. H. ARDRON
CEGB, Berkeley Nuclear Laboratories, Berkeley, Gloucestershire, U.K.

(*Received* 10 *October* 1977)

Abstract—One-dimensional two-fluid equations are used to calculate the mass flux of initially saturated or subcooled water discharging from a pipe in critical flow. The model allows in a general way for thermal non-equilibrium between the liquid and vapour bubbles, and for interphase relative motion.

The theory is shown to be in good agreement with the measured critical flow-rates of pressurised water over a wide pressure range for a single choice of parameters characterising (i) the density of nucleation sites in the liquid, (ii) the liquid superheat required to cause bubble nucleation.

Predictions are made of the critical mass flux of initially saturated water in pipes of the range of sizes of interest in water-reactor blowdown safety analysis. Results indicate that for pipes up to ten diameters in length flows will be significantly higher than values obtained from conventional homogeneous thermal equilibrium flow theory.

1. INTRODUCTION

Accurate prediction of the critical flow-rate of a steam–water mixture in a pipe is a problem of fundamental importance in the blowdown safety analysis of water cooled nuclear reactors.

Over the past 20 years there have been many experimental studies of critical vapour–liquid flow in pipes and nozzles, and several models have been proposed to account for observations. Reviews of this work by Simon (1973) and Ardron & Furness (1976) show that none of the available models provides a satisfactory description of the effects on the critical flow rate of variations in the length and diameter of the flow passage. Discrepancies, which often become large when the discharge pipe is short, are usually due to a failure to correctly represent interphase thermal non-equilibrium and interphase relative motion. Critical flow measurements have not so far been possible for reactor-size pipes. Deficiencies in the models can therefore lead to substantial uncertainties in the discharge flow-rate assumed in a reactor blowdown safety calculation.

The objective of this paper is to develop a physical model for the critical flow of initially saturated or subcooled liquid which can describe accurately the observed effects of pipe length and diameter on flow-rate.

Calculations are based on the use of one-dimensional two-fluid equations (Ishii 1975) to describe the acceleration of the boiling two-phase mixture in the pipe. In contrast to previous work, which has usually been based on the homogeneous flow model, (e.g. Simpson & Silver 1962; Edwards 1968; Malnes 1975) this representation allows interphase relative motion to be included naturally in the analysis. The model includes a treatment of the delayed nucleation and growth of vapour bubbles, and of the effects of friction and area change.

Predictions of the new model are compared with available data for a range of pressures, and the theory is used to calculate the critical mass flux of saturated water in wide-bore pipes of interest in reactor blowdown calculations.

2. OUTLINE OF METHOD OF CALCULATION

Critical vapour–liquid flow in a pipe is characterised by a steepening pressure gradient which becomes extremely large at the choking plane (Isbin *et al.* 1962; Zaloudek 1964). Simpson & Silver (1962) showed that for real boiling liquids this behaviour would be expected even in the absence of friction, as a consequence of the acceleration of the flow caused by delayed vapour generation. In the steady state the flow-rate adjusts itself so that the choking plane coincides

with the pipe exit, in order to satisfy the conservation laws. This suggests that a possible way of calculating the critical mass flux in a pipe of given size is to vary the assumed flow-rate until the choking plane is predicted to coincide with the end of the pipe. This method, which was first used for calculating critical flow-rates by Edwards (1968), has been used in the calculations described below.

The position of the choking plane for an assumed mass flow-rate in a duct of arbitrary size is determined by solving one-dimensional equations of the two-fluid model (Ishii 1975). The rate of mass transfer is determined by considering the nucleation and growth of vapour bubbles in the superheated liquid. Momentum transfer between phases is calculated from standard relations for the viscous and inertial drag on small spherical gas bubbles. It is assumed that bubbles do not coalesce, and that the thermal boundary layers surrounding individual bubbles do not interact.

The major simplifying assumption is the representation of the axisymmetric flow in the pipe, and inlet region, using a one-dimensional approximation. Thus the flow in a tapering or constant-area pipe is calculated using area-averaged forms of the conservation equations: in a similar way flow in the reservoir upstream of a pipe inlet is calculated assuming a uniformly converging radial flow.

3. CONSERVATION EQUATIONS

The conservation equations used are based on the general two-fluid equations derived by Ishii (1975). Simplifications are introduced by considering an adiabatic, one-dimensional flow, and averaging the equations across the duct area. For steady conditions the equations for conservation of mass and momentum of phase k are, neglecting body forces,

$$\left.\begin{aligned} u_k\rho_k\frac{d\alpha_k}{d\eta}+\alpha_k u_k\frac{d\rho_k}{d\eta}+\alpha_k\rho_k\frac{du_k}{d\eta}&=\Gamma_k-\alpha_k\rho_k u_k\frac{1}{A_\eta}\frac{dA_\eta}{d\eta}\\ (p_k-p_{ki})\frac{d\alpha_k}{d\eta}+\alpha_k\rho_k u_k\frac{du_k}{d\eta}+\alpha_k\frac{dp_k}{d\eta}&=(u_{ki}-u_k)\Gamma_k+\tau_{kd}+\tau_{kw}\end{aligned}\right\} \quad [1]$$

where u_k, p_k, ρ_k, and α_k denote respectively the velocity, pressure, density and volumetric concentration of phase k at axial position η in the duct. Γ_k is the rate of increase of mass of phase k per unit mixture volume due to phase change, and τ_{kd}, τ_{kw} represent the drag force on phase k per unit mixture volume due respectively to interfacial and wall shear. A_η is the duct area at position η. The variables subscripted ki are properties of phase k in the neighbourhood of the interface. Throughout the paper k will refer either to the gas phase $k \equiv G$, or the liquid phase $k \equiv L$.

Equations [1] incorporate the conventional simplifying assumption that averages of products of dependent variables across the duct are identical to products of averages.

Anticipating that we will wish to calculate the rate of formation and growth of individual bubbles we introduce a time coordinate $t(\eta)$ as an additional dependent variable. $t(\eta)$, is defined as the time taken for a typical bubble to reach position η from some initial location where the flow is nearly stationary. It must satisfy the kinematic equation:

$$\frac{dt}{d\eta}=u_G^{-1}. \quad [2]$$

4. CONSTITUTIVE AND STATE EQUATIONS

Before [1] and [2] can be integrated, constitutive relations are required to define the interfacial conditions, and the rates of interphase mass- and momentum-transfer.

4.1 *Interfacial conditions*

It is assumed (i) that liquid inertia and surface tension have a negligible influence on the growth of vapour bubbles and (ii) that the liquid adjacent to the interface remains saturated. Thus

$$p_{Gi} = p_{Li} = p_G = p_L, \tag{3}$$

and

$$T_{iL} = T_{SAT}(p). \tag{4}$$

For steam and water [3] is a reasonable assumption for bubble growth over the timescales of tens of milliseconds of interest here (e.g. Board & Duffey 1971). Equation [4] can likewise be shown to be valid for pressure changes occurring over times greater than a few microseconds (Ardron & Duffey 1977).

For simplicity the mean flow velocity at the interface is taken as the bulk average velocity of the liquid. Hence

$$u_{Gi} = u_{Li} = u_L. \tag{5}$$

4.2 *State equations*

It is assumed that the vapour is a perfect gas and obeys the saturated vapour pressure law obtained by integrating the Clausius–Clapeyron equation. Neglecting the vapour density compared with the liquid density this becomes:

$$\ln p + h_{GL} \cdot \frac{\rho_G}{p} = \text{const.} \tag{6}$$

where R_G is the gas constant for unit mass of the vapour and h_{GL} is the latent heat. The liquid is taken as incompressible so that:

$$\rho_L = \text{const., independent of temperature.} \tag{7}$$

4.2.1 *Evaporation rates.* Prediction of the evaporation rate Γ_G in boiling requires a determination of both the rate of appearance of bubbles, and of their subsequent growth. Simplified models for these processes are described below.

(a) Nucleation rates. In practical boiling systems bubble nuclei formation is assisted by the action of impurities, undissolved gases etc. in the liquid, and by nucleation sites in the container walls. Such heterogeneous constituents allow boiling to take place for liquid superheats which are orders of magnitude smaller than those required to boil pure liquids (e.g. Cole 1974). Kinetic theory arguments suggest that in the presence of solid impurities the rate of formation of bubble nuclei per unit liquid mass is given by a relation of the form (Hirth & Pound 1963):

$$\frac{dn_b}{dt} = \bar{\nu} n_s \exp(-\psi w_n/\beta T_L). \tag{8}$$

Here n_s is the effective density of heterogeneous nucleation sites in the liquid and $\bar{\nu} = (2\sigma_L R_G/\pi\beta)^{1/2}$ is a frequency factor connected with the impingement flux of liquid molecules. β is the Boltzmann constant and σ_L the liquid surface tension. The factor $\psi(\leqslant 1)$ depends on the surface geometry, and on the angle of contact with which the liquid wets the solid. w_n is the Gibbs energy of formation of the nucleus in a pure liquid, which if the vapour inside the nucleus is assumed to be at the saturation pressure $p_{SAT}(T_L)$ is given by:

$$w_n = 16\pi\sigma_L^3/3[p - p_{SAT}(T_L)]^2. \tag{9}$$

Equations [8] and [9] imply that the liquid superheat must exceed some critical value before appreciable nucleation can take place. By using the linearised Clausius–Clapeyron equation it is straightforward to show that this so-called "incipient boiling superheat" is given by (e.g. Cole 1974)

$$\theta_c = T_L - T_{SAT} = \frac{T_{SAT}}{\rho_G h_{GL}} \left[\frac{16\pi\sigma_L{}^3\psi}{3\beta T_L \ln(n_s\bar{\nu})} \right]^{1/2} \quad [10]$$

where T_{SAT} is the saturation temperature at the ambient pressure. Equation [10] is obtained by setting $dn_b/dt = 1$ in [8]. Eliminating ψ between [8] and [10], noting that $\theta_c \ll T_L = T_{SAT}$, and that $n_s \ll \bar{\nu}$ in most examples of heterogeneous nucleation, the nucleation rate can be expressed in terms of θ_c by the relation

$$\frac{dn_b}{dt} = n_s\bar{\nu} \exp\left\{ - \frac{\rho_G{}^2 h_{GL}^2 (\ln\bar{\nu})\theta_c{}^2}{T_L{}^2[p - p_{SAT}(T_L)]^2} \right\}. \quad [11]$$

As noted above a practical boiling system contains a range of agents to assist nucleation, each of which presumably has an associated activation energy ψw_n, and site density n_s. However, direct measurements of heterogeneous nucleation rates in boiling are not available at present. In their absence the assumption is made that [11] can describe the average nucleation rate due to all processes combined, provided a suitable choice is made for adjustable parameters n_s and θ_c. An essentially similar procedure was used with reasonable success by Simpson & Silver (1962) and Rohatgi & Reshotko (1975) for calculating transient boiling rates in accelerating vapour–liquid mixtures.

(b) Rate of bubble growth. The rate at which vapour forms inside a bubble depends on the heat flux in the liquid at the bubble wall, q_{iL}. Applying an energy balance to a control volume surrounding a single spherical vapour bubble of radius $R_b(t)$ we get the usual growth relation (Plesset & Zwick 1954):

$$\frac{d}{dt}\left[\frac{4}{3}\pi R_b{}^3\rho_G\right] = \frac{q_{iL}}{h_{GLi}} \cdot 4\pi R_b{}^2, \quad [12]$$

where h_{GLi} is the latent heat of the saturated liquid at the interface.

For the expansion of initially saturated or subcooled water in a duct the calculations of section 6.3 suggest that the velocity of bubbles relative to the surrounding liquid is usually small. It is therefore assumed that heat transfer from the liquid to the bubble takes place mainly by diffusion. A detailed calculation of the diffusive heat flux, allowing for the sphericity and motion of the bubble wall, is not justified in view of the simple formulation used to predict bubble number density. As a first approximation, effects of sphericity are neglected, the interface being treated as a plane. Following Carslaw & Jaeger (1959) we then have, assuming the liquid temperature T_L outside the bubble thermal boundary layers is constant,

$$q_{iLD}(t, t') = -\operatorname{Limit}_{x\to 0} \frac{\partial}{\partial x}\left\{ \frac{x\epsilon_L}{(4\pi D_L)^{1/2}} \int_{t'}^{t} \frac{T_{iL}(t'') - T_L}{(t - t'')^{3/2}} \exp\left\{ \frac{-x^2}{4D_L(t - t'')} \right\} dt'' \right\}, \quad [13]$$

where $q_{iLD}(t, t')$ refers to the diffusive heat flux at t in the wall of a bubble created at t'. x is the distance from the interface on the liquid side, and ϵ_L and D_L denote respectively the thermal conductivity and thermal diffusivity of the liquid.

In the problem of present interest the interface temperature $T_{iL} = T_{SAT}$ (c.f. [4]) decreases monotonically as the elapsed time t increases. Numerical calculations (section 6) show that the variation of pressure and temperature experienced by a bubble travelling along the pipe have the form shown schematically in figure 1. For a bubble appearing at t' the simplest ap-

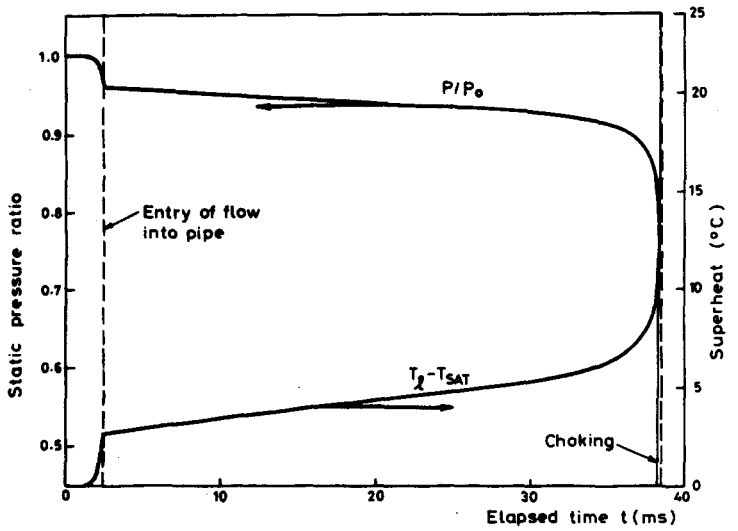

Figure 1. Variation of pressure and liquid superheat as two-phase mixture accelerates along a pipe. (Based on results of numerical calculations for 70 bar steam–water flow).

proximation to the time variation in $T_{SAT} - T_L$ is a linear function of the form

$$\theta(t) = \theta(t') + \text{const.}\,(t - t') \qquad [14]$$

where $\theta(t) \equiv T_L - T_{SAT} \cdot \theta(t')$ is the liquid superheat at bubble inception. Inspection of figure 1 suggests that the linear approximation [14] describes the variation in liquid superheat adequately for the growth of the majority of bubbles. The approximation is weakest in the region of rapidly changing pressure gradient near the choking plane. However, since the object of the present calculation is to determine the location of the choking region rather than its detailed structure, this deficiency is considered acceptable.

With this linear approximation the integration in [13] can be performed analytically giving:

$$q_{iLD}(t, t') = \frac{\epsilon_L}{\sqrt{\pi D_L (t - t')}}[2\theta(t) - \theta(t')]. \qquad [15]$$

Inserting this expression for the heat flux into [12], and integrating, again adopting the linear approximation [14] for the superheat, we get the following approximate relation for the radius at time t of a bubble created at t':

$$R_b(t, t') = R_b(t', t') + \frac{2\epsilon_L (t - t')^{1/2}}{3h_{GLi}\rho_G (\pi D_L)^{1/2}}[2\theta(t) + \theta(t')]. \qquad [16]$$

The evaporation rate $\Gamma_G(t)$ is found by summing over all bubbles formed in unit volume of the two-phase mixture up to an elapsed time t:

$$\Gamma_G(t) = \rho_L h_{GLi}^{-1} \int_0^t \left(\frac{dn_b}{dt}\right)[1 - \alpha_G(t')] q_{iLD}(t, t') 4\pi R_b^2(t, t')\, dt'. \qquad [17]$$

Substituting for (dn_b/dt), q_{iLD}, R_b from [11], [15] and [16], and neglecting the radius of a newly created nucleus compared with its radius at later times, we get the equation:

$$\Gamma_G(t) = n_s C \int_0^t e^{-g(t')}(1 - \alpha_G)(t - t')^{1/2}\{2\theta(t) + \theta(t')\}^2\{2\theta(t) - \theta(t')\}\, dt' \qquad [18]$$

where:

$$C = 16\bar{\nu}\epsilon_L^3\rho_L/(9\pi^{1/2}h_{GLi}^3\rho_G^2 D_L^{3/2})$$

$$g(t) = \rho_G^2 h_{G1}^2\theta_c^2 \ln \bar{\nu}/\{T_L^2[p_{SAT}(T_L) - p(t)]^2\}.$$

Equation [18] can be used for initially subcooled flows, provided the integrand is understood to be zero for the subcooled portion of the expansion, for which $p > p_{SAT}(T_L)$.

4.2.2 *Momentum transfer rates.* (a) Wall shear effects. For high velocity bubbly flow in a circular duct it is usual to relate the mean pipe wall shear stress S_w to the mass flow-rate W using an empirical equation of the form (Wallis 1969):

$$S_w = \frac{f_F W^2}{(2\pi^2\rho_m R_D^4)}, \qquad [19]$$

where $\rho_m = \alpha_G\rho_G + \alpha_L\rho_L$, is the mean density of the two-phase mixture, R_D is the pipe radius, and f_F is an appropriate single phase flow friction factor. For turbulent flow in the fully rough flow regime, which is the condition most usually of interest here, a suitable empirical relation for f_F is (Streeter 1961):

$$f_F^{-1/2} = 3.48 + 4.0\log_{10}(R_D/e). \qquad [20]$$

We take the roughness as $e = 45 \times 10^{-6}$ m, a value typically quoted for steel pipes.

In bubbly flow there is no direct contact between the vapour and the walls of the pipe. It is therefore reasonable to assume that:

$$\left.\begin{aligned} \tau_{Gw} &= 0 \\ \tau_{Lw} &= -2S_w/R_D = -f_F W^2/(\pi^2\rho_m R_D^5) \end{aligned}\right\} \qquad [21]$$

where S_w has been eliminated using [19].

(b) Inter-phase momentum transfer. Following Ardron & Duffey (1977) the drag force on a cluster of small spherical bubbles in unit volume of an accelerating bubbly mixture is written:

$$\tau_{Gd} = -\tau_{Ld} = \frac{-9\alpha_G\mu_L(u_G - u_L)}{2\bar{R}_b^2} - \frac{\rho_L\alpha_G(1+2\alpha_G)}{2(1-\alpha_G)}u_G\left[\frac{du_G}{d\eta} - \frac{du_L}{d\eta}\right] \qquad [22]$$

where μ_L is the liquid viscosity. This equation is applicable to a steady flow. The first term on the right hand side corresponds to the Stokes viscous drag; the second term arises from the inertial drag on the bubble due to its virtual mass.

At any position in the duct bubbles of a range of sizes are present. An average radius for use in [22] is calculated using the formula:

$$\bar{R}_b(t) \approx [3\alpha_G/(4\pi n_v(t))]^{1/3}, \qquad [23]$$

$n_v(t)$, the volume concentration of bubbles in the two-phase mixture, is given by integrating [11]:

$$n_v(t) = n_s\bar{\nu}\rho_L\int_0^t [1 - \alpha_G(t')]\,e^{-g(t')}\,dt', \qquad [24]$$

where $g(t)$ is defined after [18].

5. NUMERICAL CALCULATIONS OF CRITICAL FLOW-RATES

5.1 *Matrix form of equations*

It follows from the saturated vapour pressure law [6] that:

$$\frac{d\rho_G}{d\eta} = \left[\frac{\rho_G}{p} - \frac{1}{h_{GL}}\right]\frac{dp}{d\eta}. \qquad [25]$$

Eliminating τ_{kd}, τ_{kw} using [21] and [22], and using [3], [5], [7] and [25] the mass and momentum conservation relations [1], and the kinematic equation [2], can be combined in a matrix form

$$A\, d\mathbf{y}/d\eta = \mathbf{b}, \qquad [26]$$

where:

$$\mathbf{y}^T = (\alpha_G, t, p, u_G, u_L).$$

The elements of the square matrix A, and the column vector $\mathbf{b}$, are given in the appendix. A one-dimensional approximation to the flow-field in a duct of arbitrary geometry can be calculated by integrating [26] with a suitable choice for the duct area terms in $\mathbf{b}$.

5.2 *Pipe geometry*

For the illustrative calculations and data comparisons of section 6 we consider vapour–liquid flow in constant area pipes with both tapering and radiused inlets. These are illustrated in figure 2.

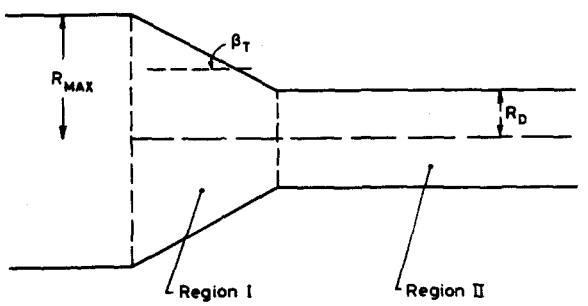

(a) Pipe with Conical Tapering Inlet.

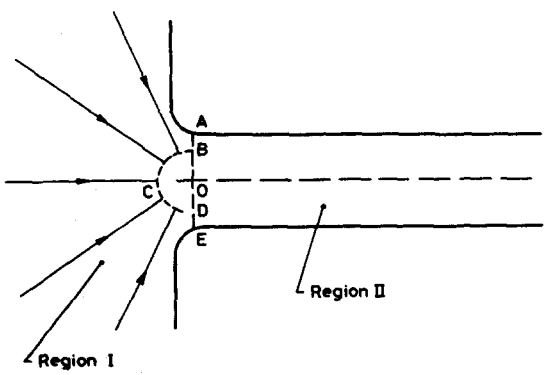

(b) Pipe with Radiused Inlet.

Figure 2. Pipe inlet configurations considered in critical flow calculations.

In the constant area section the flow-field is straightforwardly represented by [26], if we take $dA_\eta/d\eta = 0$. For flow in entrance the following formulations were adopted:

(a) *Tapering inlet.* Flow in the converging passage (region I of figure 2a) was in this case calculated by putting

$$A_\eta^{-1}\, dA_\eta/d\eta = -2 \tan \beta_T/(R_{max} - \eta \tan \beta_T)$$

where β_T is the half angle of the conical taper and R_{max} its largest radius.

(b) *Radiused inlet.* The flow field in the entry region (region I of figure 2b) was treated as radial and inviscid, with path lines converging towards point 0. This radial field can be represented by [26] if we take

$$A_\eta^{-1}\, dA_\eta/d\eta = 2/\eta,$$

and replace η by the radial co-ordinate measured from 0. The boundary conditions for the flow in the pipe were specified by matching conditions on the entry plane (*ABODE*) to those on the hemisphere *BCD* in region I, whose surface area is the full pipe area; this preserves the continuity of the dependent variables α, ρ_G, u_k, t in passing between regions I and II.

5.3 *Solution procedure*

The differential equations [26] were integrated by a predictor–corrector method in the computer programme CRACKPOT. Details of the method of solution are given in the appendix. As outlined in section 2, above, the choked flow-rate is calculated by:

(i) postulating a flow-rate, W;

(ii) integrating the [26] along the pipe, starting at a point in the entrance region where the flow is almost stationary;

(iii) determining the distance from the pipe entrance L^* at which the pressure gradient becomes arbitrarily large (the limit used in the numerical calculation was $dp/d\eta >$ 50 bar/mm). L^* is the length of pipe consistent with the postulated choked flow-rate W.

6. RESULTS AND DISCUSSION

6.1 *Comparison of the theory with experimental data*

The theory compared with available measurements of the critical flow-rate of subcooled and saturated water at high pressures. A best fit to the range of data examined in the present work was obtained by setting the nucleation site density n_s equal to 1000/kg and taking the incipient boiling superheat as $\theta_c = 3.0$°C. We note that direct measurements of nucleation rates in boiling could be used to confirm these values, and thus provide an independent check of the nucleation model used here.

Figure 3 gives an indication of the sensitivity of the predicted mass flux G^* to variations in n_s and θ_c. Illustrative calculations are given for the flow of saturated water in 20 mm dia. radiused entry pipes at a pressure of 70 bar. It is seen that the predicted mass flux is insensitive to variations of n_s within a factor of two. Predictions depend more strongly on the choice for θ_c, and the determination of an optimum value required more careful examination of data.

The critical flow-rate of initially saturated and subcooled water in a 254 mm long 12.8 mm dia. pipe was measured by Zaloudek (1964) for stagnation pressures in the range $20 < p_0 <$ 100 bar. In these experiments the inlet section consisted of a 36 mm long conical taper, with an included angle of $2\beta_T = 20°$. Test results are compared with model predictions in figure 4 (data below the broken line are for two-phase entry conditions, which are outside the range of validity of the present model), h_0 denotes the liquid enthalpy in the reservoir. Agreement between the experiment and theory is seen to be good.

Sozzi & Sutherland (1975) measured the critical flow-rate of saturated and subcooled water

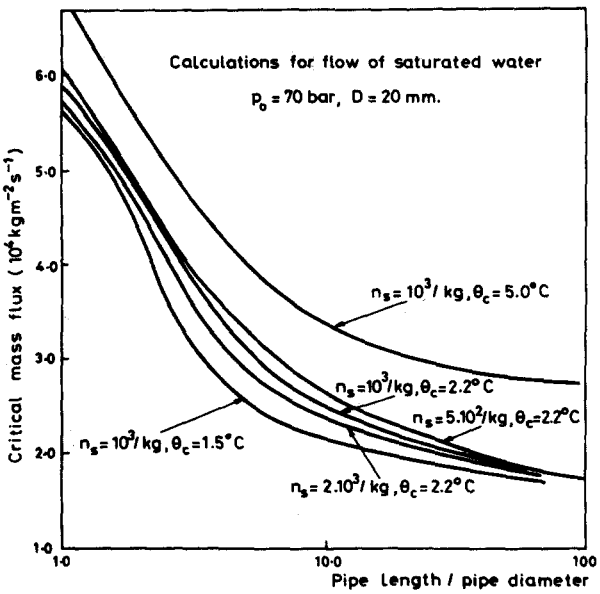

Figure 3. Sensitivity of calculated critical mass flux to choice of parameters n_s and θ_c.

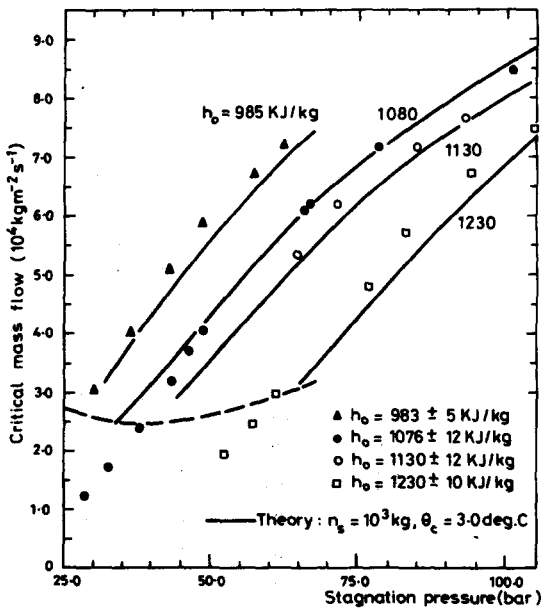

Figure 4. Comparison of theory with Zaloudek's (1964) data. Pipe with a tapering inlet.

in 12.7 mm dia. radiused entry pipes, up to 1.8 m long. Reservoir pressures were in the range $55 < p_0 < 75$ bar. The present theory is compared with the saturated-water data in figure 5, and with subcooled water data in figure 6. Also shown in figure 5 is the critical mass flux determined assuming isentropic homogeneous equilibrium flow. It is seen that predictions fall mostly within the scatter on the experimental results, providing encouraging support for the model.

The critical flow-rates of initially saturated water in 6.35 mm dia. pipes were measured over a wide range of stagnation pressures $5 < p_0 < 150$ bar in tests conducted by Fauske (1965). In these experiments the pipes had sharp-edged entries. Earlier experiments by Bailey (1952) suggest that in high velocity steam–water flow separation downstream of sharp-edged entrance will result in an annular flow pattern, in which a stable vapour cavity surrounds a low void fraction two-phase jet; the latter can travel many diameters before expanding to fill the pipe.

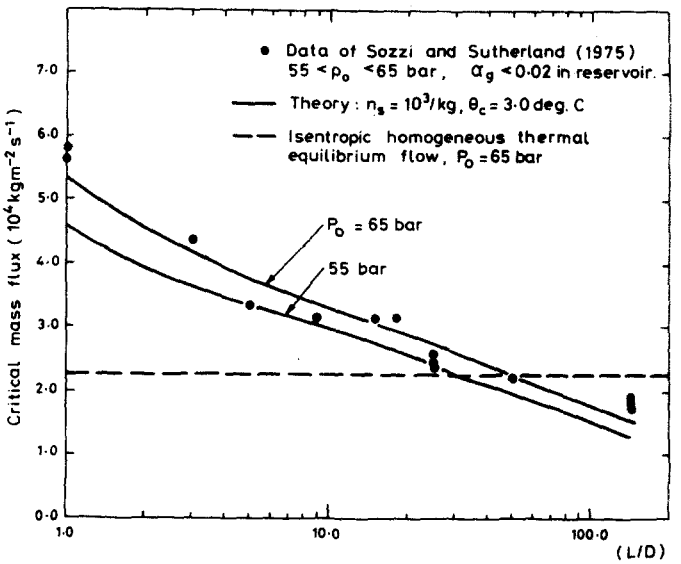

Figure 5. Comparison of theory with the measured critical mass flux of saturated water in radiused entry 12.7 dia. pipes.

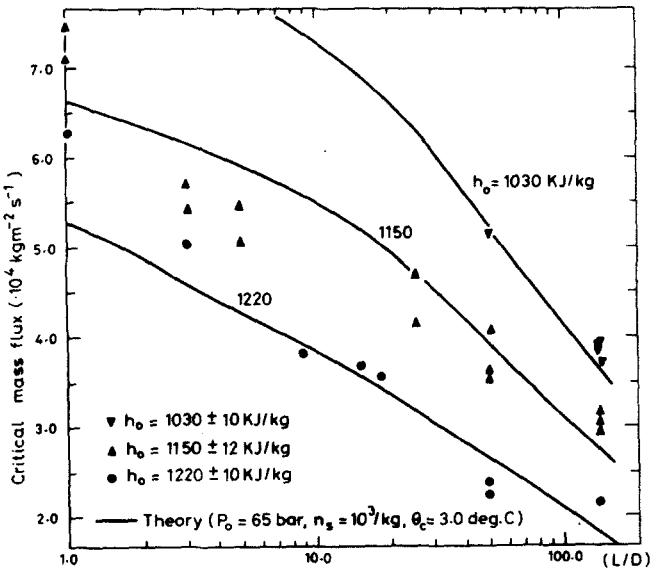

Figure 6. Comparison of theory with the measured critical mass flux of subcooled water in radiused entry 12.7 mm dia. pipes.

Such behaviour could not be represented by the present model, which ignores both separation and details of the flow pattern. However, inlet effects presumably become negligible for very long pipes. In figure 7 the present model is compared with G^* measured in the longest pipes of Fauske's test series, $L/D = 40$. Agreement is within 10% over the experimental pressure range, and within the scatter on the results. However there is a noticeable systematic under-prediction of flows at high pressures. It is interesting that the data fall close to predictions of isentropic thermal equilibrium flow theory. This agreement, is however, fortuitous, since the assumption of frictionless flow is seriously in error for the long narrow bore pipe used in these tests.

6.2 *Variation of velocity and pressure along the pipe*

It is interesting to examine in more detail the calculated axial velocity and pressure profiles in a pipe carrying a critical vapour–liquid flow.

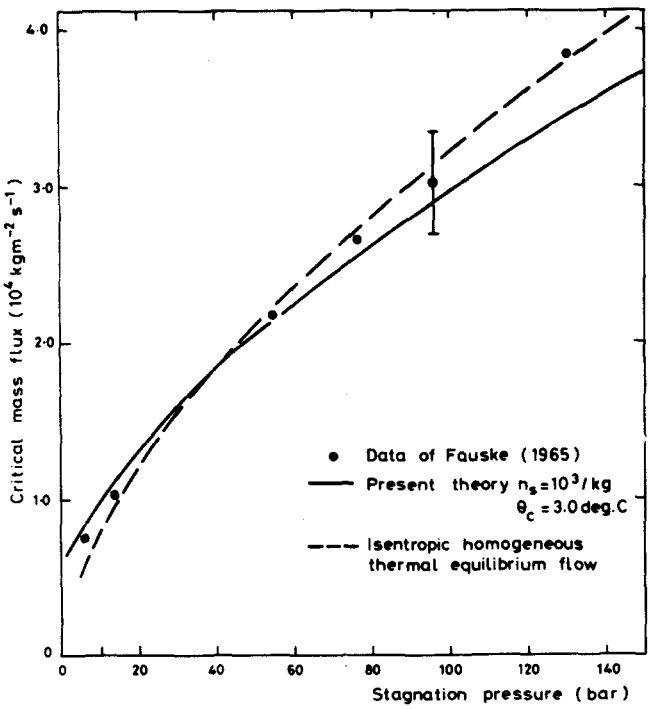

Figure 7. Comparison of theory with the measured critical mass flux of saturated water in a square-edged entry pipe, length $L = 254$ mm, diameter $D = 6.35$ mm.

Figure 8a shows the predicted velocity profile for a typical example. It is seen that interphase relative motion is only significant in the entrance to the pipe and in the large pressure gradients near the exit, where the velocity ratio u_G/u_L rises to ~ 1.1. In the calculations reported in this paper the value of the velocity ratio in the exit region was never observed to exceed 1.25. Interphase acceleration is inhibited by the virtual mass of the bubbles and by the large viscous drag which is a consequence of their small size. In the example shown the average bubble radius 100 mm upstream of the choking plane was calculated as 0.015 mm. The bubble number density at the same position was calculated as $8 \times 10^{12}/\text{m}^3$.

In the neighbourhood of the choking plane the phase velocities u_G and u_L we always found to be close to the local sound speed

$$C_{D\infty} \doteqdot \sqrt{\frac{\rho_G C_G^2}{\alpha_G(1-\alpha_G)\rho_L}\left\{1+\frac{2\alpha_G(1-\alpha_G)^2}{1+2\alpha_G}\right\}}$$

obtained by linearising the governing two-fluid equations. Here C_G is the velocity of sound in the vapour. As discussed by Ardron & Duffey (1977) this agreement is consistent with the conventional view of choking as a condition in which downstream pressure changes cannot be transmitted across the critical plane.

Figure 8b shows the two-phase pressure drop for the same example. Also shown is the pressure gradient calculated by assuming a homogeneous thermal-equilibrium flow, retaining pipe wall friction. It is seen that non-equilibrium effects can have a dominating influence on the position of the choking plane, and on the static pressure gradient, is a pipe carrying a critical vapour–liquid flow.

6.3 *Calculation of the critical-flow in wide bore pipes*

The model was used to compute the critical mass flux of initially saturated water in wide-bore radiused entry pipes. Results plotted in figure 9(a,b) show the independent effects of

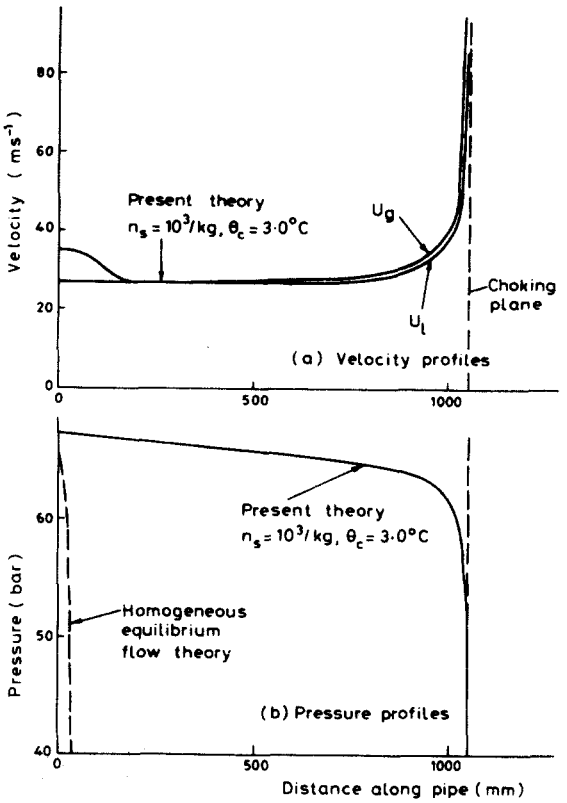

Figure 8. Predicted variation in fluid velocity and pressure along a pipe in the critical flow of saturated water. ($G^* = 2.0 \times 10^4$ kg^{-1}s^{-1}, $p_0 = 70$ bar).

pipe length and diameter on G^*. Also shown are predictions conventional isentropic homogeneous equilibrium flow theory. Several interesting points emerge from these comparisons:

(i) significant effects of non-equilibrium are indicated for pipes less than ten diameters long, even for pipes of very wide bore;

(ii) G^* is predicted to vary strongly with pipe length, and only weakly with pipe diameter;

(iii) it is predicted that for a fixed length of pipe, G^* has a weak maximum at some critical pipe diameter. This is attributable to the competing effects of flow friction and interphase non-equilibrium on G^*. Friction tends to depress the mass flux as the diameter of a fixed length of pipe is reduced. Non-equilibrium effects tend, on the other hand, to increase G^*, and these become more important as D is reduced so that the transit time of fluid particles from the reservoir to the pipe exit becomes shorter. The existence of a maximum mass flux for a fixed length of pipe was predicted qualitatively by Simon (1973); the present model provides quantitative estimates of this effect.

7. CONCLUSIONS

A two-fluid model for nonequilibrium vapour–liquid flow has been used to calculate the mass flux of initially saturated or subcooled water discharging from a pipe in critical flow. The theory is in good agreement with data over a wide range of reservoir pressures for a single choice of parameters characterising (i) the density of nucleation sites in the liquid, and (ii) the liquid superheat required to cause bubble nucleation. Measurements of heterogenous nucleation rates in boiling are desirable to confirm these values, and provide independent support for the model.

Calculations suggest that in the critical flow of a high pressure bubbly steam–water mixture the average velocity of the furrounding liquid exceeds that of the bubbles by more than about

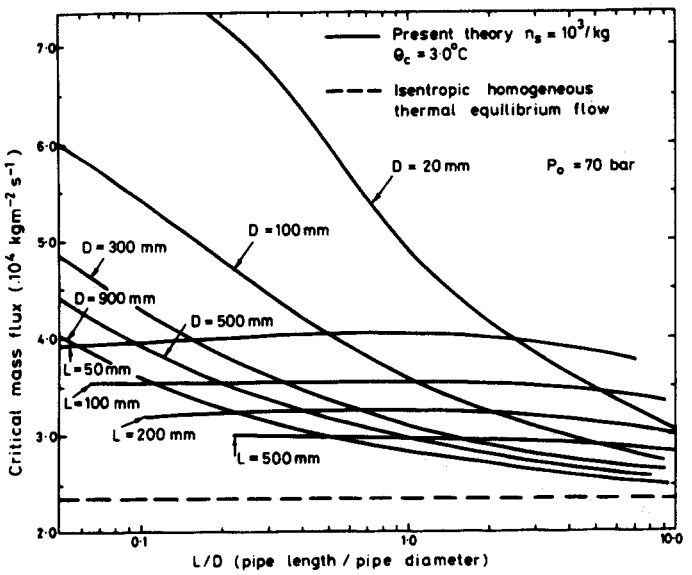

Figure 9a. Predicted critical mass flux of initially saturated water in large bore pipes for $p_0 = 70$ bar.

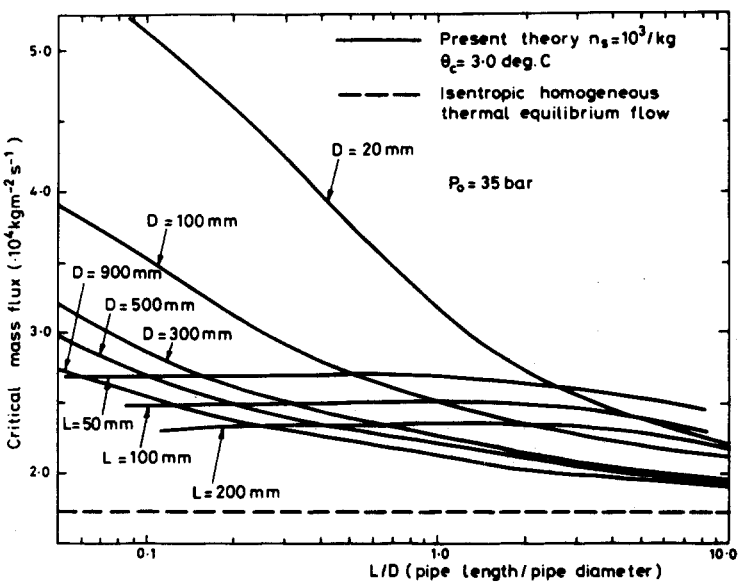

Figure 9b. Predicted critical mass flux of initially saturated water in large bore pipes for $p_0 = 35$ bar.

twenty-five per cent, even in the large pressure gradients near the pipe exit. Velocities near the exit are predicted to be close to the velocity of sound waves of high frequency.

The model has been used to calculate the critical flow-rate of saturated water in pipes of the range of sizes of interest in water-reactor blowdown safety analysis. Results suggest that the discharge flow in pipes up to ten diameters in length can be significantly larger than values obtained from homogeneous thermal equilibrium flow theory.

It is predicted that because of the competing effects of thermal non-equilibrium and pipe wall friction on flow-rate the critical mass flux in a given length of pipe will be a maximum for a particular pipe diameter.

Acknowledgement—This paper is published by permission of the Central Electricity Generating Board.

REFERENCES

ARDRON, K. H. & DUFFY, R. B. 1977 Acoustic wave propagation in a flow liquid–vapour mixture. *Int. J. Multiphase Flow* **4**, 303–322.

ARDRON, K. H. & FURNESS, R. A. 1976 A study of critical flow models used in reactor blowdown analysis. *Nucl. Engng Design* **39**, 257–266.

BAILEY, J. F. 1951 Metastable flow of saturated water. *Trans ASME* **13**, 1109–1116.

BOARD, S. J. & DUFFEY, R. B. 1971 Spherical bubble growth in superheated liquids. *Chem. Engng Sci.* **26**, 263–274.

CARSLAW, M. S. & JAEGER, J. C. 1959 *Conduction of Heat in Solids*, pp. 62–64. Oxford University Press, Oxford.

COLE, R. 1974 Boiling nucleation. *Adv. Heat Transf.* **10**, 85–166.

EDWARDS, A. R. 1968 Conduction controlled flashing of a fluid, and the prediction of critical flow rates in a one-dimensional system. UKAEA Report AHSB(S) R147.

FAUSKE, H. K. 1965 The discharge of saturated water through tubes. *Chem. Engng Prog. Symp. Ser.* **61**, 211–216.

HIRTH, J. P. & POUND, G. M. 1963 Condensation and evaporation: nucleation and growth kinetics. *Prog. Materials Sci.* 11.

ISBIN, H. S., FAUSKE, H. K., GRACE, T. & GARCIA, I. 1962 Two-phase steam–water pressure drops for critical flows. *Proc. Instn Mech. Engrs. Symp. Two-Phase Flow* 81–92.

ISHII, M. 1975 *Thermo-Fluid Dynamic Theory of Two-Phase Flow*. Eyrolles, Paris.

MALNES, D. 1975 Critical two-phase flow based on non-equilibrium effects, in *Non-Equilibrium Two-Phase Flows* (Edited by LAHEY, R. T. & WALLIS, G. B.), Vol. 11.18. Am. Society Mech. Engrs., New York.

PLESSET, M. S. & ZWICK, S. A. 1954 The growth of vapour bubbles in superheated liquids. *J. Appl. Phys.* **25**, 493–500.

ROHATGI, U. S. & RESHOTKO, E. 1975 Non-equilibrium one-dimensional two-phase flow in variable area channels, in *Non-Equilibrium Two-Phase Flows* (Edited by LAHEY, R. T. & WALLIS, G. B.), pp. 47–54. Am. Society Mech. Engrs., New York.

SIMON, U. 1973 Blowdown flowrates of initially saturated water, Topical Mtg. on Water-Reactor Safety, pp. 172–195. Salt Lake City, CONF.-73034.

SIMPSON, H. C. & SILVER, R. S. 1962 Theory of one-dimensional two-phase homogeneous non-equilibrium flow. Proc. Inst. Mech. Engrs. Symp. Two-Phase Flow, pp. 45–56.

SOZZI, G. L. & SUTHERLAND, W. A. 1975 Critical flow of saturated and subcooled water at high pressures, G.E. Report HW-13418.

STREETER, V. L. (Ed.) 1961 *Handbook of Fluid Dynamics*, Vol. 3, p. 16. McGraw-Hill, New York.

WALLIS, G. B. 1969 *One-Dimensional Two-Phase Flow*. McGraw–Hill, New York.

ZALOUDEK, F. R. 1964 The critical flow of hot water through short tubes. G.E. Report HW-77594, Hanford Labs.

APPENDIX

Notes on the numerical procedure used to integrate [26]

The form of the square matrix A and column vector $\mathbf{b}$ in [26] are as follows:

$$\mathbf{b} = \begin{bmatrix} \Gamma_G - \alpha_G \rho_{GSAT}(p) u_G A_\eta^{-1} \, dA_\eta/d\eta \\ -\Gamma_G - (1-\alpha_G)\rho_L u_L A_\eta^{-1} \, dA_\eta/d\eta \\ \Gamma_G(u_L - u_G) - \xi \\ \xi - 2S_w/R_D \\ u_G^{-1} \end{bmatrix}$$

$$A = \begin{bmatrix} u_G\rho_{GSAT}(p) & 0 & \alpha_G u_G\left[\dfrac{\rho_{GSAT}(p)}{\rho} - \dfrac{1}{h_{GL}}\right] & \alpha_G\rho_{GSAT}(p) & 0 \\ -\rho_L u_L & 0 & 0 & 0 & (1-\alpha_G)\rho_L \\ 0 & 0 & \alpha_G & \zeta + \alpha_G u_G \rho_{GSAT}(\rho) & -\zeta \\ 0 & 0 & (1-\alpha_G) & -\zeta & [\zeta + (1-\alpha_G)\rho_L u_L] \\ 0 & 1 & 0 & 0 & 0 \end{bmatrix}$$

where $\rho_{GSAT}(p)$ denotes the density of saturated vapour at pressure p and we have used the additional notation:

$$\zeta = \frac{\alpha_G}{2}\rho_L u_G\left(\frac{1+2\alpha_G}{1-\alpha_G}\right)$$

$$\xi = \frac{9\alpha_G\mu_L(u_G - u_L)}{2\bar{R}_b^2},$$

and the facts that

$$\alpha_G = (1-\alpha_L); \quad \Gamma_G = -\Gamma_L.$$

Equation [26] was solved by a finite-difference method in the computer program CRACKPOT. Solution is achieved by dividing the flow field into a series of mesh points $\eta_1 \ldots \eta_{i-1}$, η_i, $\eta_{i+1} \ldots$ etc. In the interval $[\eta_j, \eta_{j+1}]$ the equation is integrated by a standard predictor-corrector method assuming the evaporation rate, Γ_G, and the mean bubble radius, R_b, maintain the values they possess at point η_j. Evaluation of conditions at η_{j+1} allows Γ_G and R_b to be re-calculated, and the solution thus proceeds to the next mesh point.

To calculate Γ_G and R_b at the kth spatial step the integrals in [18] and [24] were replaced by the finite difference formulae:

$$\Gamma_G^{(k)} = \frac{1}{2}n_s C \sum_{j=1}^{j=k-1}[\phi_{k,j} + \phi_{k,j+1}][t^{(j+1)} - t^{(j)}]$$

$$n_b^{(k)} = \frac{1}{2}n_s\bar{v}\rho_L \sum_{j=1}^{j=k-1}[\mu_j + \mu_{j+1}][t^{(j+1)} - t^{(j)}],$$

where:

$$\phi_{k,j} = [t^{(k)} - t^{(j)}]^{1/2}[2\theta^{(k)} + \theta^{(j)}]^2[2\theta^{(k)} - \theta^{(j)}]\mu_j$$

$$\mu_j = [1 - \alpha_G^{(j)}]\exp[-g^{(j)}].$$

The superscript (j) etc. denotes the value of a dependent variable at position $\eta^{(j)}$.

Mesh spacing was reduced until convergence within a suitable tolerance had been achieved. Typically several hundred mesh points were required to give reasonable accuracy.